Automatic prostate cancer detection through DCE-MRI images: all you need is a good normalization

Guillaume Lemaître, MS[a,b,*], Robert Martí, PhD[b], Mojdeh Rastgoo, PhD[a],
Joan Massich, PhD[a], Jordi Freixenet, PhD[b], Anke Meyer-Baese, PhD[d],
Joan C. Vilanova, MD[c], Fabrice Meriaudeau, PhD[a,e]

[a]*LE2I UMR6306, CNRS, Arts et Métiers, Univ. Bourgogne Franche-Comté, 12 rue de la Fonderie, 71200 Le Creusot, France*
[b]*ViCOROB, Universitat de Girona, Campus Montilivi, Edifici P4, 17071 Girona, Spain*
[c]*Department of Magnetic Resonance, Clínica Girona, Lorenzana 36, 17002 Girona, Spain*
[d]*Department of Scientific Computing, 400 Dirac Science Library, Florida State University, Tallahassee, FL 32306, United States*
[e]*CISIR, Electrical & Electronic Engineering Department, Universiti Teknologi Petronas, 32610 Seri Iskandar, Perak, Malaysia*

Abstract

Purpose multiparametric Magnetic Resonance Imaging (MRI) (mp-MRI) plays a major role in the detection of Prostate Cancer (PCa) and is commonly used to the design of new Computer-Aided Detection and Diagnosis (CAD) systems. Dynamic Contrast-Enhanced (DCE)-MRI is one of the modality regularly used in mp-MRI CAD system. Pharmocokinetric parameters are extracted from the DCE-MRI sequences and later used to discriminate cancerous from healthy tissue. However, some inter-patients variations occur during the data acquisition leading to estimation errors of the pharmacokinetic parameters. Therefore, we propose a fully automatic normalization method for DCE-MRI that reduces the inter-patient variability of the data.

---

*Corresponding author.
Email address: g.lemaitre58@gmail.com (Guillaume Lemaître, MS)

Materials and Methods The inter-patient variations in DCE-MRI are corrected based on a graph-based intensity offsets correction as well as a time offset and data dispersion correction. This normalization is applied ahead of usual pharmacokinetic quantitative analysis. The different parameters are used in a Random Forest (RF) classifier in order to distinguish cancerous voxels from healthy one.

Results The best classification performance to detect PCa is obtained using the whole DCE-MRI normalized signal, reaching an Area Under the Curve (AUC) of 0.666 ($\pm$0.154) and outperforming the quantitative approaches.

Conclusion We show the benefit of our normalization method prior to extract quantitative and semi-quantitative features, with a significant improvement of the classification performance. Nevertheless, we also show that using the whole normalized DCE-MRI signal outperforms all quantitative approaches.

Keywords: DCE-MRI, prostate cancer, normalization, classification, quantification

1. Introduction

Prostate Cancer (PCa) is the second most frequently diagnosed men cancer, accounting for 899,000 cases leading to 258,100 deaths [1]. As highlighted by the PI-RADS Steering Committee, the two main challenges to be addressed are [2]: (i) the improvement of detecting clinically significant PCa and (ii) an increase of the confidence in benign or dormant cases, avoiding

2

unnecessary invasive medical exams. In this regard, multiparametric Magnetic Resonance Imaging (MRI) (mp-MRI) is frequently used to build robust Computer-Aided Detection and Diagnosis (CAD) systems to detect, localize, and grade PCa. In general, CAD systems are based on mp-MRI which potentially combines several of the following modalities [3]: T_2 Weighted (T_2-W)-MRI, Dynamic Contrast-Enhanced (DCE)-MRI, Apparent Diffusion Coefficient (ADC) maps, and Magnetic Resonance Spectroscopy Imaging (MRSI).

In DCE-MRI, a contrast media is injected intravenously and a set of images is acquired over time. Consequently, each voxel in an image corresponds to a dynamic signal which is related to both contrast agent concentration and the vascular properties of the tissue. Therefore, changes of the enhanced signal allows to discriminate healthy from PCa tissues. In fact, these properties are automatically extracted using quantitative or semi-quantitative approaches [3].

Quantitative approaches uses pharmacokinetic modelling based on a bi-compartment model, namely Brix [4] and Tofts [5] models. The parameters of the Brix model are inferred assuming a linear relationship between the media concentration and the MRI signal intensity. This assumption has shown, however, to lead to inaccurately estimate the pharmacokinetic parameters [6]. In the contrary, Tofts model requires a conversion from MRI signal intensity to concentration, which becomes a non-linear relationship using specific equation of MRI sequences (e.g., FLASH sequence). Tofts modelling suffers, however, from a higher complexity [7]. Indeed, the conversion using the non-linear approach requires to acquire a T_1 map which is not always possible during clinical examination. Additionally, the parameter

3

calculation requires the Arterial Input Function (AIF) which is challenging to measure and can also lead to an inaccurate estimation.

Semi-quantitative approaches are rather mathematical than pharmacokinetic modelling since no pharmacokinetic assumption regarding the relation between the MRI signal and the contrast agent are made [8, 7]. These methods offer the advantages to not require any knowledge about the MRI sequence nor any conversion from signal intensity to concentration. However, they present some limitations: the heuristic approach proposed by Huisman et al. requires an initial estimate of the noise standard deviation of the signal as well as some manual tuning.

Nevertheless, all presented methods suffer from two major drawbacks: (i) inter-patient variability and (ii) loss of information. The inter-patient variability is mainly due to the acquisition process and consequently leads to generalization issue while applying a machine learning algorithm. All previous methods extract few discriminative parameters to describe the DCE-MRI signal which might lead to a loss of information.

In this work, we propose a fully automatic normalization method for DCE-MRI that reduces the inter-patient variability of the data. The benefit and simplicity of our approach will be shown by classifying the whole normalized DCE-MRI signal and comparing with the state-of-the-art quantitative and semi-quantitative methods. Additionally, we will show that using this normalization approach in conjunction with the quantitative methods improves the classification performance of most of the models. We also propose a new clustering-based method to segment enhanced signals from the arteries, later used to estimate an AIF as well as an alternative approach to

4

estimate the parameters of the semi-quantitative model proposed by [8].

The paper is organized as follows: Section 2.1 gives information about the dataset used and provided source code. Section 2.2 details our normalization strategy for DCE-MRI data. Quantitative and semi-quantitative methods are summarized in Sect. 2.3 with insights about their implementations. Experiments and results to answer the previous stated challenges are reported in Sect. 3 while discussed in Sect. 4, followed by a concluding section.

2. Material and Methods

2.1. MRI data

The multi-parametric MRI data are acquired from a cohort of patients with higher-than-normal level of Prostate-Specific Antigen (PSA). The acquisition is performed using a 3T whole body MRI scanner (Siemens Magnetom Trio TIM, Erlangen, Germany) using sequences to obtain T_2-W-MRI, DCE-MRI and Diffusion Weighted (DW)-MRI. Aside of the MRI examination, these patients also have undergone a guided-biopsy. The dataset is composed of a total of 20 patients of which 18 patients have biopsy proven PCa and 2 patients are "healthy" with negative biopsies. Therefore, 13 patients have a PCa in the Peripheral Zone (PZ), 3 patients have PCa in the Central Gland (CG), 2 patients have invasive PCa in both PZ and CG and finally 2 patients are considered as "healthy". An experienced radiologist has segmented the prostate organ — on T_2-W-MRI and DCE-MRI — as well as the prostate zones (i.e., PZ and CG) and PCa on the T_2-W-MRI.

A 3 mm slice fat-suppressed T_2-W fast spin-echo sequence (Repetition Time (TR)/Echo Time (TE)/Echo Train Length (ETL): 3400 ms/85 ms/13)

5

is used to acquire images in sagittal and oblique coronal planes, the latter planes being orientated perpendicular or parallel to the prostate PZ rectal wall axis. Three-dimensional T_2-W fast spin-echo (TR/TE/ETL: 3600 ms/143 ms/109, slice thickness: 1.25 mm) images are then acquired in an oblique axial plane. The nominal matrix and Field Of View (FOV) of the 3D T_2-W fast spin-echo images are 320×256 and 280×240 mm^2, respectively, thereby affording sub-millimetric pixel resolution within the imaging plane.

DCE-MRI is performed using a fat suppressed 3D T_1 VIBE sequence (TR/TE/Flip angle: 3.25 ms/1.12 ms/10°; Matrix: 256×192; FOV: 280×210 (with 75% rectangular FOV); slab of 16 partitions of 3.5 mm thickness; temporal resolution: 6 s/slab over approximately 5 min). A power injector (Medrad, Indianola, USA) is used to provide a bolus injection of Gd-DTPA (Dotarem, Guerbet, Roissy, France) at a dose of 0.2 ml Gd-DTPA/kg of body weight.

These DCE-MRI sequences are resampled using the spatial information of the T_2-W-MRI and missing data are interpolated using a linear interpolation. The volumes of the DCE-MRI dynamic are rigidly registered, to remove any patient motion during the acquisition. Furthermore, a non-rigid registration is performed between the T_2-W-MRI and DCE-MRI in order to propagate the prostate zones and PCa ground-truths.

The resampling is implemented in C++ using the Insight Segmentation and Registration Toolkit [9]. The implementation of the registration (C++), normalization (Python), and classification pipeline (Python) are publicly

6

available on GitHub[1] [10]. The data used for this work are also publicly available[2] [11].

2.2. Normalization of DCE-MRI images

In this work, we propose a method to normalize DCE-MRI prostate data to reduce inter-patient variations, although it can be applied to any DCE-MRI sequences. In T_2-W-MRI, these variations are characterized by a shift and a scaling of the intensities as illustrated by the intensity Probability Density Function (PDF) in Fig. 1. Therefore, these variations can be corrected using a z-score approach— i.e., normalizing the data by subtracting the mean and dividing by the standard deviation —assuming that the data follow a specific distribution [12].

In DCE-MRI, the intensity PDF of prostate gland does not follow a unique type of distribution such as Rician or Gaussian distribution, as shown in Fig. 2(a). Indeed, the inter-patient variations are more complex due to the temporal acquisition. A better representation to observe these variations is to represent the intensity PDF of the prostate gland over time— requiring to segment the prostate —using a heatmap representation as shown in Fig. 2(a). Analyzing this heatmap representation across patients (see Fig. 2(c)), the following variations are highlighted: (i) intensity offsets Δ_i of the PDF peak, (ii) a time offset Δ_t depending of the contrast agent arrival, and (iii) a change of scale α_i related to the signal enhancement. Therefore, our normalization method should attenuate all these variations and be performed globally across

---

[1]https://github.com/I2Cvb/lemaitre-2016-nov/tree/master
[2]https://zenodo.org/record/61163

7

the different time sequences rather than for each independent sequence.

2.2.1. Graph-based intensity offsets correction

Before to standardize each sequence, the first step of the normalization
is to cancel the intensity specific at each patient, occurring due to the media
injection. As previously mentioned, the intensity PDF does not always follow
either a Rician or a Gaussian distribution over time, in DCE-MRI. Therefore,
the mean of these distributions cannot be used as a potential estimate for
these offsets. Additionally, these offsets should be characterized by a smooth
transition between series over time. Thus, this problem is solved using the
graph-theory: considering the intensity PDF over time as shown in Fig. 2(a),
the offsets correspond to the boundary splitting the heatmap in two partitions
such that they are as close as possible to the peak of the intensity PDF (see
Fig. 3 for an illustration). Given the heatmap, a directed weighted graph
$\mathcal{G} = (\mathcal{V}, \mathcal{E})$ is built by taking each bar— i.e., the probability for a given
time and pixel intensity—of the heatmap as a node and connecting each
pair of bars by an edge. The edge weight w_{ij} between two nodes i and j
corresponding to two pixels at position (x_i, y_i) and (x_j, y_j), respectively, is
defined as in Eq. (1):

$$w_{ij} = \begin{cases} \alpha \exp(1 - \frac{H(i)}{\max(H)}) & \text{if } x_j = x_i + 1 \text{ and } y_j = y_i, \\ (1 - \alpha) \exp(1 - \frac{H(i)}{\max(H)}) & \text{if } x_j = x_i \text{ and } y_j = y_i + 1, \\ 0 & \text{otherwise,} \end{cases} \quad (1)$$

where H is the heatmap, α is a smoothing parameter controlling the parti-
tioning.

8

Therefore, these offsets related to Δ_i are estimated by finding the shortest-path to cross the graph using Dijkstra's algorithm. The entry and exiting nodes are set to be the bin with the maximum probability for the first DCE-MRI serie and the bin corresponding to the median value for the last DCE-MRI serie, respectively. To ensure a robust estimation of these offsets, the process of finding the shortest-path is iteratively repeated by shifting the data and updating the heatmap as well as the graph $\mathcal{G}$. The procedure is stopped once the offset found does not change. In general, this process is not repeated more than 3 iterations. The parameter α is set to 0.9, empirically. Figure 3 illustrates the final estimation of the offsets Δ_i (i.e., red landmark) found for each DCE-MRI serie. Therefore, each intensity offset is subtracted for each DCE-MRI.

2.2.2. Time offset and data dispersion correction

The next variations to correct are the time offset Δ_t and the data dispersion σ_i. By computing the Root-Mean-Square Deviation (RMSD) of the intensities for each DCE-MRI serie, one can observe these two variations as shown in Fig. 4(a). Therefore, to correct these variations, we propose to register each patient RMSD to a mean model which corresponds to the mean of all patients RMSD. The parametric model to perform the registration is formulated as in Eq. (2):

$$T(\alpha, \tau, f(t)) = \alpha f(t - \tau), \qquad (2)$$

where α and τ are the two parameters handling the time offset Δ_i and global

scale σ_i, respectively, $f(\cdot)$ is the RMSD function define as:

$$f(t) = \sqrt{\left(\frac{\sum_{n=1}^{N} x(t)_n^2}{N}\right)}, \tag{3}$$

where $x(t)_n$ is the shifted intensity of a sample from a specific DCE-MRI serie at time t from a total number of N samples.

Therefore the registration problem is equivalent to:

$$\arg\min_{\alpha,\tau} = \sum_{t=1}^{N} \left[T\left(\alpha, \tau, f(t)\right) - \mu(t)\right]^2, \tag{4}$$

where $\mu(\cdot)$ is the mean model, N is the number of DCE-MRI serie.

Illustration of the correction applied to each RMSD patient is shown in Fig. 4(b). Once all these parameters have been inferred, the data are shifted as well as scaled.

The resulting normalized data can be used into two fashions: (i) each normalized signal can be used as a whole to determine whether the corresponding voxel is healthy or cancerous or (ii) the normalized data can be fitted using a quantitative method, as presented in the next section.

2.3. Quantification of DCE-MRI

In this section, we summarize the different methods which have been used for the quantification of DCE-MRI for PCa detection [3] and which will be used for comparison in this work. Furthermore, we would like to emphasize the following additional contributions for this section: (i) a novel automatic AIF estimation algorithm based on clustering and (ii) a simplified semi-quantitative method using constrained optimization.

2.3.1. Brix and Hoffmann models

In the Brix model [4], the MRI signal intensity is assumed to be proportional to the media concentration. Therefore, the model is expressed as in Eq. (5):

$$s_n(t) = 1 + A\left[\frac{\exp(k_{el}t') - 1}{k_{ep}(k_{ep} - k_{el})}\exp(-k_{el}t) - \frac{\exp(k_{ep}t') - 1}{k_{el}(k_{ep} - k_{el})}\exp(-k_{ep}t)\right], \quad (5)$$

with

$$s_n(t) = \frac{s(t)}{S_0}, \quad (6)$$

where $s(t)$ and S_0 are the MRI signal intensity at time t and the average pre-contrast MRI signal intensity, respectively; A, k_{el}, and k_{ep} are the constant proportional to the transfer constant, the diffusion rate constant, and the rate constant, respectively. Additionally, t' is set such that $0 \leqslant t \leqslant \tau$, $t' = t$ and afterwards while $t > \tau$, $t' = \tau$.

Hoffmann et al. proposed a similar model as expressed in Eq. (7), which derive from the Brix model:

$$s_n(t) = 1 + \frac{A}{\tau}\left[\frac{k_{ep}\left(\exp(k_{el}t') - 1\right)}{k_{el}(k_{ep} - k_{el})}\exp(-k_{el}t) - \frac{\exp(k_{ep}t') - 1}{(k_{ep} - k_{el})}\exp(-k_{ep}t)\right], \quad (7)$$

in which the constant A is redefined by isolating the parameter τ.

The parameters A, k_{el}, and k_{ep} are estimated by fitting the model using non-linear least-squares optimization solved with Levenberg-Marcquardt.

11

2.3.2. Tofts model

The extended Tofts model is formulated as in Eq. (8):

$$C_t(t) = K_{trans}C_p(t) * \exp(-k_{ep}t) + v_pC_p(t), \qquad (8)$$

where $*$ is the convolution operator; $C_t(t)$ and $C_p(t)$ are the concentrations
of contrast agent in the tissue and in the plasma, respectively; K_{trans}, k_{ep},
and v_p are the volume transfer constant, the diffusion rate constant, and the
plasma volume fraction, respectively.

Therefore, Tofts model requires to: (i) detect candidate voxels from the
femoral or iliac arteries and estimate a patient-based AIF signal, (ii) convert
the MRI signal intensity (i.e., AIF and dynamic signal) to a concentration,
and (iii) in the case of a population-based AIF, estimate an AIF signal.

Segmentation of artery voxels and patient-based AIF estimation The
AIF signal from DCE-MRI can be manually estimated by selecting the
most-enhanced voxels from the femoral or iliac arteries [14]. Few meth-
ods have been proposed to address the automated extraction of AIF
signal. Chen et al. filtered successively the possible candidates to be
considered as AIF such that [15]: (i) dynamic signals with small peak
and voxels with a small wash-in are rejected by thresholding, (ii) a blob
detector is used and large enough regions are kept, and (iii) circular and
cylindricality criteria are used to reject the false positives. Zhu et al.
proposed an iterative method selecting voxels which best fit a gamma
variate function [16]. However, it requires to compute first and second
derivatives as well as maximum curvature points. Shanbhag et al. pro-
posed a 4-steps algorithm [17, 18]: (i) remove slices with artefacts and

12

find the best slices based on intrinsic anatomic landmarks and enhancement characteristics, (ii) find the voxel candidates using the maximum enhanced voxels and a multi-label maximum entropy based thresholding algorithm, (iii) exclude region next to the endorectal coil, and (iv) select the best 5 candidates which meet enhancement characteristics and that are correlated.

All the above methods are rather complex and thus we propose a simpler method which is based on the following reasonable assumptions: (i) all possible AIF signal candidates should have a similar shape, (ii) a high enhancement, and (iii) the arteries should be almost round and within a size range. Therefore, each slice is clustered into regions using K-means clustering with $k = 6$. The cluster made of the most enhanced signals is selected since it contains the artery signals. In this regards, the selection criteria corresponds to the 90th percentile of the maximum DCE-MRI signal. Finally, regions with an eccentricity smaller than 0.5 and an area in the range of $[100, 400]$ voxels are kept. Additionally, to remove voxels contaminated by partial volume effect, only the 10% most enhanced voxels of the possible candidates are kept as proposed by [19] and the average signal is computed. A summary of the different segmentation steps is presented in Fig. 5.

Conversion of MRI signal intensity to concentration To estimate the free parameters of the Tofts model (see Eq. (8)), the concentration $C_t(t)$ and $C_p(t)$ need to be computed from the MRI signal intensity and the AIF signal, respectively. This conversion is based on the equation of the FLASH sequence—see Appendix A for details—and is formulated

13

as in Eq. (9):

$$c(t) = \frac{1}{TR \cdot r_1} \ln \left(\frac{1 - \cos \alpha \cdot S^* \frac{s(t)}{S_0}}{1 - S^* \frac{s(t)}{S_0}} \right) - \frac{R_{10}}{r_1}, \tag{9}$$

with,

$$S^* = \frac{1 - \exp(-TR \cdot R_{10})}{1 - \cos \alpha \cdot \exp(-TR \cdot R_{10})}, \tag{10}$$

where $s(t)$ is the MRI signal, S_0 is the MRI signal prior to the injection of the contrast media, α is the flip angle, TR is the Repetition Time (TR), R_{10} is the pre-contrast tissue relaxation time also equal to $\frac{1}{T_{10}}$, and r_1 is the relaxitivity coefficient of the contrast agent.

T_{10} can be estimated from the acquisition of a T_1 map. However, this modality is not part of the clinical trial in this research and the value of T_{10} is fixed to 1600 ms for both blood and prostate, in accordance with the values found in the literature [18, 20, 21].

Estimation of population-based AIF While estimating the pharmacokinetic parameters from Tofts model, the AIF concentration $C_p(t)$ can be computed either from the patient or a population. We presented in the two previous sections the algorithms which allows to estimate the patient-based AIF concentration. To compare with the previous approach, we also computed a population-based AIF which will be also used later to compare the performance of both approaches. In that regard, the population-based AIF was estimated as in [14] by fitting the average patient-based AIFs to the model of [22] which is formulated as in Eq. (11):

$$C_p(t) = \sum_{n=1}^{2} \frac{A_n}{\sigma_n \sqrt{2\pi}} \exp \left(\frac{-(t - T_n)^2}{2\sigma_n^2} \right) + \frac{\alpha \exp(-\beta t)}{1 + \exp -s(t - \tau)}, \tag{11}$$

14

where A_n, T_n, and σ_n are the scaling constants, centers, and widths of the nth Gaussian, α and β are the amplitude and decay constant of the exponential; and s and τ are the width and center of the sigmoid function, respectively.

The parameters are estimated by fitting the model using a constrained non-linear least-squares optimization, solved with the Trust Region Reflective algorithm [23] and bounding the parameters to be positive.

2.3.3. PUN model

Gliozzi et al. showed that Phenomenological Universalities (PUN) approach can be used for DCE-MRI analysis [7]. The model has been successfully used in a CAD system proposed by [24]. This model can be expressed as in Eq. (12):

$$s_n(t) = \exp\left[rt + \frac{1}{\beta}\left(a_0 - r\right)\left(\exp(\beta t) - 1\right)\right],\tag{12}$$

with

$$s_n(t) = \frac{s(t) - S_0}{S_0},\tag{13}$$

where $s(t)$ and S_0 are the MRI signal intensity at time t and the average pre-contrast MRI signal intensity, respectively; r, a_0, and β are the free parameters of the model.

The parameters are estimated by fitting the model using non-linear least-squares optimization solved with Levenberg-Marcquardt.

15

2.3.4. Semi-quantitative analysis

The semi-quantitative analysis of the DCE-MRI is equivalent to extracting curve characteristics directly from the signal without a strict theoretical pharmacokinetic meaning. In this work, we use the model presented by [8] which formulated the MRI signal as in Eq. (14):

$$
s(t) = \begin{cases}
S_0 & 0 \leqslant t \leqslant t_0 \\
S_M - (S_M - S_0) \exp\left(\frac{-(t-t_0)}{\tau}\right) & t_0 < t \leqslant t_0 + 2\tau \\
S_M - (S_M - S_0) \exp\left(\frac{-(t-t_0)}{\tau}\right) + w(t - t_0 + 2\tau) & t > t_0 + 2\tau
\end{cases}
\tag{14}
$$

where $s(t)$ is the MRI signal intensity, S_0 is the pre-contrast signal intensity, t_0 is the time corresponding to the start of enhancement, S_M and τ is the maximum of the signal and the exponential time constant, and w is the slope of the linear part.

Huisman et al. argue that curve fitting via least-squares minimization using Nelder-Mead algorithm leads to inaccurate estimation of the free parameters: mainly the issue come from an incorrect estimation of the start of enhancement t_0 leading to incorrect estimation of the other parameters. Therefore, they propose to: (i) estimate robustly t_0, (ii) estimate S_0 by averaging the samples between 0 and t_0 (ii) estimate w depending if the slope is significant or not, (iii) estimate S_M which should be the point at the intersection of the most probable slope line and the plateau.

Instead of these successive estimations, we propose a unified optimization in which t_0 is fixed since that this is a key parameter. Therefore, t_0 is robustly estimated from the AIF signal since that this is the most enhanced signal

16

in which the start of enhancement is easily identifiable. The AIF signal is computed as in Section 2.3.2. t_0 is estimated by finding the maximum of the first derivative of the AIF signal, always occurring at the beginning of the signal. Then, the function in Eq. (14) is fitted using non-linear least squares with the Trust Region Reflective algorithm [23]. Furthermore, the parameters τ and S_M are bounded during the optimization to ensure robust estimations. τ is bounded between t_0 and t_f which is the time of the last sample while S_M is bounded between S_0 and $\max(s(t))$.

From Eq. (14), the following features are extracted: (i) the wash-in corresponding to the slope between t_0 and $t_0 + 2\tau$, (ii) the wash-out corresponding to the parameter w, (iii) the area under the curve between t_0 and the end of the signal, (iv) the exponential time constant τ, and (v) the relative enhancement $S_M - S_0$.

3. Results

3.1. Goodness of model fitting

Parameter estimation of the quantification methods are related to fit a specific model to the DCE-MRI data. Therefore, this section report the goodness of fitting by computing the coefficient of determination R^2 such as in Eq. (15)

$$R^2 = 1 - \frac{\sum_{t=1}^{T}(s_t - \hat{s}_t)^2}{\sum_{t=1}^{T}(s_t - \bar{s})^2}, \tag{15}$$

where s_t and $\hat{s}_t$ are the signal to be fitted and the estimated signal at time t, respectively; $\bar{s}$ is the average signal to be fitted.

17

Mean and standard-deviation of the coefficient of determination R^2 is reported in Table 2 for each quantification model. Brix, Hoffmann, and Tofts models are fitted with a coefficient R^2 superior to 0.80. Additionally, the proposed PUN model does not seem to fit well the data. Data normalization improves the coefficient R^2 for all the methods apart of the Hoffmann model. The large standard deviation for this model might imply that there are some cases where the fitting fails.

3.2. Detection of PCa using pharmacokinetic parameters

To study the potential benefit of our normalization, PCa are detected at a voxel level using pharmacokinetic parameters estimated from un-normalized and normalized DCE-MRI data. Each individual pharmacokinetic parameter is classified to evaluate their individual discriminative power to detect PCa. Therefore, a Random Forest (RF) classifier is used in conjunction with a Leave-One-Patient-Out Cross-Validation (LOPO CV). The use of RF is motivated since that it leads to the best performance in the state-of-the-art methods [25, 3]. Results are summarized in Table 1 in terms of Area Under the Curve (AUC). Normalization can improve the detection of PCa; however, the benefit of normalization is more obvious by combining together the pharmacokinetic features of a given model (e.g., A, $k_e p$, and $k_e l$ for Brix model), as previously done in traditional CAD system [3]. For the latter configuration, results are summarized by performing a Receiver Operating Characteristic (ROC) analysis and computing the AUC, as reported in Fig. 6. Quantification using normalized data outperforms quantification using un-normalized data in terms of classification performance apart of Hoffmann and Tofts population-based AIF models. The reasons behind the decrease

18

of the AUC might be related to: (i) a poor fitting as discussed in Sect. 3.1 (cf., Hoffmann model) and (ii) a small number of patients while estimating some parameters (cf., Tofts model). The best classification performance are obtained using the semi-quantitative approach with an AUC of 0.655.

3.3. Classification of the entire enhanced DCE-MRI signal

As stated in the introduction, the quantification methods are extracting a set of parameters characterizing the enhancement DCE-MRI signal. However, this extraction might lead to a loss of information. This experiment is performed to assess if making use of the whole DCE-MRI signal instead of the just the pharmacokinetic parameters can improve the classification performance. Therefore, each enhanced DCE-MRI signal, normalized and un-normalized, is classified using a RF classifier in a LOPO CV fashion. The ROC analysis and AUC are reported in Fig. 7. Classification without normalization lead to the worst performance, with an AUC of 0.568. However, data normalization in conjunction with the use of the whole DCE-MRI signal is the strategy which outperforms all others, with an AUC of 0.666.

4. Discussions

The experiments conducted in the previous section can give rise to several discussions. In Tofts quantification, two different approaches have been used to infer the pharmacokinetic parameters: using a population-based or a patient-based AIF. The patient-based AIF approach leads to better classification performance. However, there are two shortcomings to take into account while advancing this fact: (i) T_{10} parameter has been fixed and not computed from a T_1 map and (ii) the population-based AIF has been estimated

19

from a cohort of only 17 patients. These two limitations have to be considered while advancing that population-based AIF modelling is outperforming patient-based AIF modelling.

The best classification performance is reached by normalizing the DCE-MRI data and use the whole enhanced signal as feature, emphasizing the fact that a loss of information while extracting quantitative parameters. Furthermore, this normalization is a less complex process than all quantification methods. However, this strategy suffers from one drawback: the training time of the RF classifier increases since that from 3 to 5 features, the feature space becomes a 40 dimensions space.

Nevertheless, this study is performed on a small cohort of patients using a single MRI machine. Generalizing the results of this study on a larger dataset acquired from different commercial systems have to be considered to study the robustness of the proposed approach.

5. Conclusions and future works

In this work, we presented a new method for normalizing/standardizing DCE-MRI data. This method aimed at reducing the inter-patient variations occurring during data acquisition. A graph-based approach was used to correct intensity offset in conjunction with a model-based correction to reduce time offset as well as intensity scaling. We show the benefit of our normalization method prior to extract quantitative and semi-quantitative features, with a significant improvement of the classification performance. Nevertheless, we also show that using the whole normalized DCE-MRI signal outperforms all quantitative approaches.

20

As avenues for future research, this normalization has to be part of a mp-MRI CAD system in which DCE-MRI modality needs to be combined with other complementary modalities.

Appendix A   Conversion from FLASH signal to media concentration

In this appendix, we show the demonstration used to extract the agent concentration from the MRI signal.

The signal equation in FLASH sequence [26] is defined as:

$$s(t) = S_{eq} \sin \alpha \cdot \frac{1 - \exp\left(-TR\left(R_{10} + r_1 c(t)\right)\right)}{1 - \cos \alpha \cdot \exp\left(-TR\left(R_{10} + r_1 c(t)\right)\right)}, \tag{16}$$

where $s(t)$ is the MRI signal, S_{eq} is the maximum signal amplitude of the spoiled gradient at the TE which is proportional to the Proton Density (PD), α is the flip angle, TR is the Repetition Time (TR), R_{10} is the pre-contrast tissue relaxation time also equal to $\frac{1}{T_{10}}$, r_1 is the relaxitivity coefficient of the contrast agent, and $c(t)$ is the media concentration.

Therefore, the pre-contrast signal prior to bolus injection of the media is defined as:

$$S_0 = S_{eq} \sin \alpha \cdot \frac{1 - \exp\left(-TR \cdot R_{10}\right)}{1 - \cos \alpha \cdot \exp\left(-TR \cdot R_{10}\right)}. \tag{17}$$

To simplify the demonstration, let us define:

$$A = \exp(-TR \cdot R_{10}), \tag{18}$$

$$B = \exp(-TR \cdot r_1 c(t)). \tag{19}$$

21

Let us define:

$$S^* = \frac{S_0}{S_{eq} \sin \alpha}, \tag{20}$$

$$= \frac{1 - A}{1 - A \cos \alpha}. \tag{21}$$

Thus,

$$S^* \frac{s(t)}{S_0} = \frac{S_0}{S_{eq} \sin \alpha} \frac{s(t)}{S_0}, \tag{22}$$

$$= \frac{1 - AB}{1 - AB \cos \alpha}. \tag{23}$$

Now, let us define:

$$\frac{1 - \cos \alpha \cdot S^* \frac{s(t)}{S_0}}{1 - S^* \frac{s(t)}{S_0}} = \frac{1 - \cos \alpha \left(\frac{1 - AB}{1 - AB \cos \alpha} \right)}{1 - \frac{1 - AB}{1 - AB \cos \alpha}}, \tag{24}$$

$$= \frac{1 - AB \cos \alpha - \cos \alpha (1 - AB)}{1 - AB \cos \alpha - (1 - AB)}, \tag{25}$$

$$= \frac{1 - AB \cos \alpha - \cos \alpha + AB \cos \alpha}{1 - AB \cos \alpha - 1 + AB}, \tag{26}$$

$$= \frac{1 - \cos \alpha}{AB(1 - \cos \alpha)}, \tag{27}$$

$$= \frac{1}{AB}. \tag{28}$$

Thus,

$$-TR \cdot R_{10} - TR \cdot r_1 c(t) = \ln \left(\frac{1 - \cos \alpha \cdot S^* \frac{s(t)}{S_0}}{1 - S^* \frac{s(t)}{S_0}} \right). \tag{29}$$

Therefore,

$$c(t) = \frac{1}{TR \cdot r_1} \ln \left(\frac{1 - \cos\alpha \cdot S^* \frac{s(t)}{S_0}}{1 - S^* \frac{s(t)}{S_0}} \right) - \frac{R_{10}}{r_1}. \tag{30}$$

References

[1] J. Ferlay, H.-R. Shin, F. Bray, D. Forman, C. Mathers, D. M. Parkin, Estimates of worldwide burden of cancer in 2008: Globocan 2008, International journal of cancer 127 (2010) 2893–2917.

[2] J. C. Weinreb, J. O. Barentsz, P. L. Choyke, F. Cornud, M. A. Haider, K. J. Macura, D. Margolis, M. D. Schnall, F. Shtern, C. M. Tempany, et al., Pi-rads prostate imaging–reporting and data system: 2015, version 2, European urology 69 (2016) 16–40.

[3] G. Lemaître, R. Martí, J. Freixenet, J. C. Vilanova, P. M. Walker, F. Meriaudeau, Computer-aided detection and diagnosis for prostate cancer based on mono and multi-parametric mri: A review, Computers in biology and medicine 60 (2015) 8–31.

[4] G. Brix, W. Semmler, R. Port, L. R. Schad, G. Layer, W. J. Lorenz, Pharmacokinetic parameters in cns gd-dtpa enhanced mr imaging., Journal of computer assisted tomography 15 (1991) 621–628.

[5] P. S. Tofts, B. Berkowitz, M. D. Schnall, Quantitative analysis of dynamic gd-dtpa enhancement in breast tumors using a permeability model, Magnetic Resonance in Medicine 33 (1995) 564–568.

[6] M. Heilmann, F. Kiessling, M. Enderlin, L. R. Schad, Determination of pharmacokinetic parameters in dce mri: consequence of nonlinearity between contrast agent concentration and signal intensity, Investigative radiology 41 (2006) 536–543.

[7] A. Gliozzi, S. Mazzetti, P. P. Delsanto, D. Regge, M. Stasi, Phenomenological universalities: a novel tool for the analysis of dynamic contrast enhancement in magnetic resonance imaging, Physics in medicine and biology 56 (2011) 573.

[8] H. J. Huisman, M. R. Engelbrecht, J. O. Barentsz, Accurate estimation of pharmacokinetic contrast-enhanced dynamic mri parameters of the prostate, Journal of Magnetic Resonance Imaging 13 (2001) 607–614.

[9] L. Ibanez, W. Schroeder, L. Ng, J. Cates, The itk software guide (2005).

[10] G. Lemaitre, lemaitre-2016-nov: 0.1.0, 2016. URL: `http://dx.doi.org/10.5281/zenodo.61182`. doi:`10.5281/zenodo.61182`.

[11] G. Lemaitre, R. Martí, F. Meriaudeau, DCE-MRI prostate images, 2016. URL: `http://dx.doi.org/10.5281/zenodo.61163`. doi:`10.5281/zenodo.61163`.

[12] G. Lemaitre, M. R. Dastjerdi, J. Massich, J. C. Vilanova, P. M. Walker, J. Freixenet, A. Meyer-Baese, F. Mériaudeau, R. Marti, Normalization of t2w-mri prostate images using rician a priori, in: SPIE Medical Imaging, International Society for Optics and Photonics, 2016, pp. 978529–978529. doi:`10.1117/12.2216072`.

[13] U. Hoffmann, G. Brix, M. V. Knopp, T. Heβ, W. J. Lorenz, Pharmacokinetic mapping of the breast: a new method for dynamic mr mammography, Magnetic resonance in medicine 33 (1995) 506–514.

[14] R. Meng, S. D. Chang, E. C. Jones, S. L. Goldenberg, P. Kozlowski, Comparison between population average and experimentally measured arterial input function in predicting biopsy results in prostate cancer, Academic radiology 17 (2010) 520–525.

[15] J. Chen, J. Yao, D. Thomasson, Automatic determination of arterial input function for dynamic contrast enhanced mri in tumor assessment, in: International Conference on Medical Image Computing and Computer-Assisted Intervention, Springer, 2008, pp. 594–601. doi:10.1007/978-3-540-85988-8_71.

[16] Y. Zhu, M.-C. Chang, S. Gupta, Automated determination of arterial input function for dce-mri of the prostate, in: SPIE Medical Imaging, International Society for Optics and Photonics, 2011, pp. 79630W–79630W. doi:10.1117/12.878213.

[17] D. Shanbhag, S. N. Gupta, K. Rajamani, Y. Zhu, R. Mullick, A generalized methodology for detection of vascular input function with dynamic contrast enhanced perfusion data, in: ISMRM, volume 12, 2012, p. 10.

[18] F. M. Fennessy, A. Fedorov, T. Penzkofer, K. W. Kim, M. S. Hirsch, M. G. Vangel, P. Masry, T. A. Flood, M.-C. Chang, C. M. Tempany, et al., Quantitative pharmacokinetic analysis of prostate cancer dce-mri at 3t: comparison of two arterial input functions on cancer detection

25

with digitized whole mount histopathological validation, Magnetic resonance imaging 33 (2015) 886–894.

[19] M. C. Schabel, D. L. Parker, Uncertainty and bias in contrast concentration measurements using spoiled gradient echo pulse sequences, Physics in medicine and biology 53 (2008) 2345.

[20] C. M. De Bazelaire, G. D. Duhamel, N. M. Rofsky, D. C. Alsop, Mr imaging relaxation times of abdominal and pelvic tissues measured in vivo at 3.0 t: preliminary results 1, Radiology 230 (2004) 652–659.

[21] J. C. Carr, T. J. Carroll, Magnetic resonance angiography: principles and applications, Springer Science & Business Media, 2011.

[22] G. J. Parker, C. Roberts, A. Macdonald, G. A. Buonaccorsi, S. Cheung, D. L. Buckley, A. Jackson, Y. Watson, K. Davies, G. C. Jayson, Experimentally-derived functional form for a population-averaged high-temporal-resolution arterial input function for dynamic contrast-enhanced mri, Magnetic resonance in medicine 56 (2006) 993–1000.

[23] D. C. Sorensen, Newton's method with a model trust region modification, SIAM Journal on Numerical Analysis 19 (1982) 409–426.

[24] V. Giannini, S. Mazzetti, A. Vignati, F. Russo, E. Bollito, F. Porpiglia, M. Stasi, D. Regge, A fully automatic computer aided diagnosis system for peripheral zone prostate cancer detection using multi-parametric magnetic resonance imaging, Computerized Medical Imaging and Graphics 46 (2015) 219–226.

26

[25] G. Litjens, O. Debats, J. Barentsz, N. Karssemeijer, H. Huisman, Computer-aided detection of prostate cancer in mri, IEEE transactions on medical imaging 33 (2014) 1083–1092.

495 [26] A. Haase, J. Frahm, D. Matthaei, W. Hanicke, K.-D. Merboldt, Flash imaging. rapid nmr imaging using low flip-angle pulses, Journal of Magnetic Resonance (1969) 67 (1986) 258–266.

6. Tables

Table 1: AUC (i.e., μ ($\pm\sigma$)) for each individual pharmacokinetic parameter using a RF classifier.

Features	Un-normalized data	Normalized data
Brix model		
A	0.540 ($\pm$0.069)	0.555 ($\pm$0.080)
k_{el}	0.549 ($\pm$0.062)	0.577 ($\pm$0.093)
k_{ep}	0.506 ($\pm$0.032)	0.497 ($\pm$0.019)
Hoffmann model		
A	0.516 ($\pm$0.020)	0.508 ($\pm$0.031)
k_{el}	0.545 ($\pm$0.066)	0.529 ($\pm$0.065)
k_{ep}	0.550 ($\pm$0.063)	0.545 ($\pm$0.060)
Tofts model with population AIF		
K_{trans}	0.556 ($\pm$0.086)	0.565 ($\pm$0.097)
k_{ep}	0.506 ($\pm$0.026)	0.528 ($\pm$0.038)
v_p	0.533 ($\pm$0.064)	0.548 ($\pm$0.082)
Tofts model with patient AIF		
K_{trans}	0.563 ($\pm$0.077)	0.548 ($\pm$0.060)
k_{ep}	0.492 ($\pm$0.025)	0.491 ($\pm$0.020)
v_p	0.530 ($\pm$0.069)	0.495 ($\pm$0.033)
PUN model		
a_0	0.521 ($\pm$0.040)	0.530 ($\pm$0.045)
r	0.550 ($\pm$0.085)	0.573 ($\pm$0.097)
β	0.531 ($\pm$0.051)	0.549 ($\pm$0.068)
Semi-quantitative analysis		
wash-in	0.587 ($\pm$0.107)	0.533 ($\pm$0.032)
wash-out	0.516 ($\pm$0.037)	0.486 ($\pm$0.035)
IAUC	0.506 ($\pm$0.048)	0.513 ($\pm$0.032)
τ	0.565 ($\pm$0.104)	0.537 ($\pm$0.089)
$S_M - S_0$	0.560 ($\pm$0.083)	0.532 ($\pm$0.029)

Table 2: Coefficient of determination R^2 (i.e., μ ($\pm\sigma$)), while fitting data with the different quantification models.

Data type	Brix	Hoffmann	Tofts population AIF	Tofts patient AIF	PUN	Semi-quantitative
Un-normalized	0.85 ($\pm$0.11)	0.81 ($\pm$0.17)	0.84 ($\pm$0.14)	0.88 ($\pm$0.12)	0.27 ($\pm$0.18)	0.64 ($\pm$0.24)
Normalized	0.92 ($\pm$0.05)	0.72 ($\pm$0.32)	0.92 ($\pm$0.06)	0.90 ($\pm$0.10)	0.28 ($\pm$0.20)	0.75 ($\pm$0.20)

7. Figures

Figure 1: Illustration of the inter-patient variations in 17 different patients, using the PDF representation.

(a)

(b)

(c)
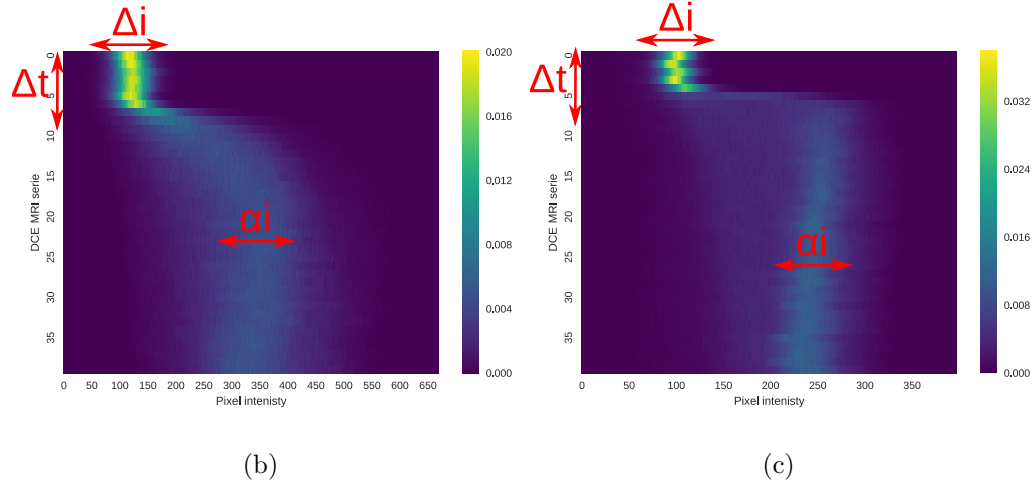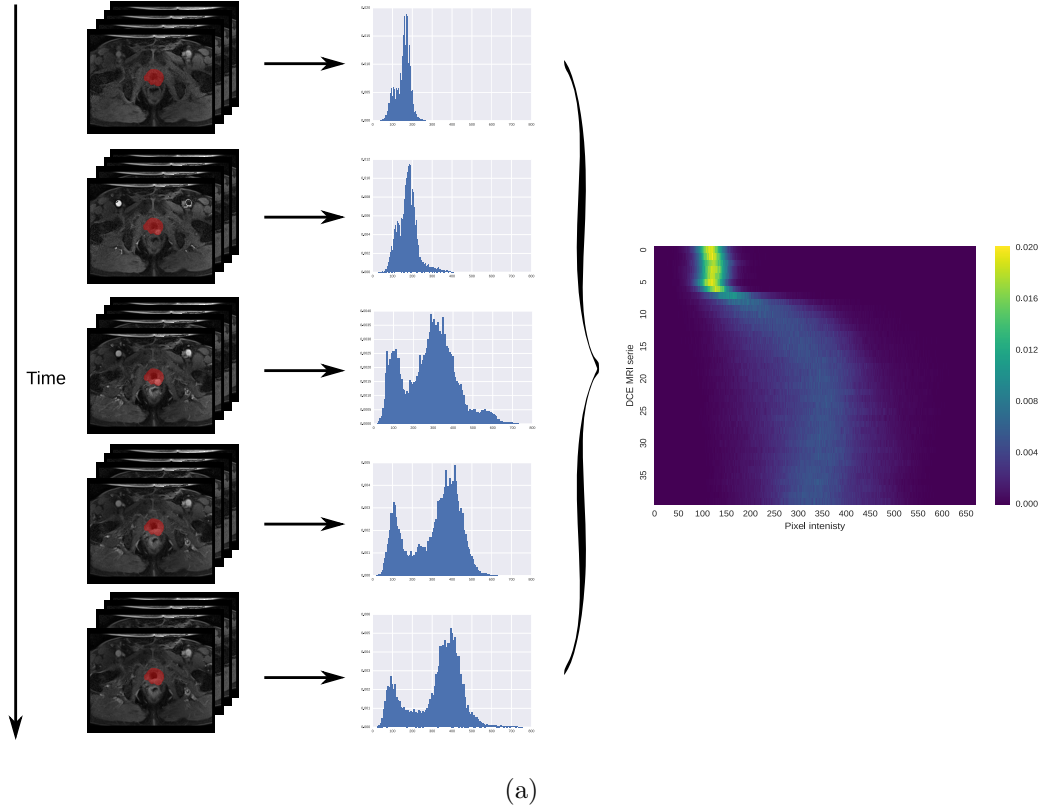
Figure 2: (a) Illustration of the heatmap representation: all PDFs of the prostate gland are concatenated together to build an heatmap; (b)-(c) Illustration of inter-patient variations (i.e., Δ_i, Δ_t, and α_i) PDF over time of two patients in a DCE-MRI.
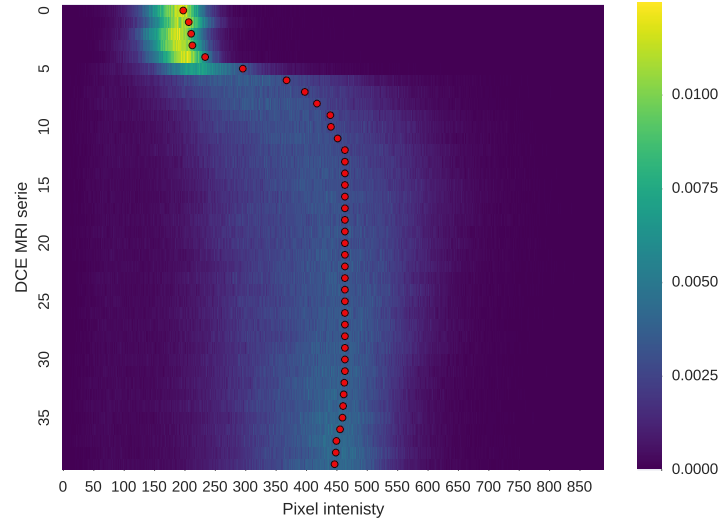
Figure 3: Illustration of the estimator found using the shortest-path through the graph.
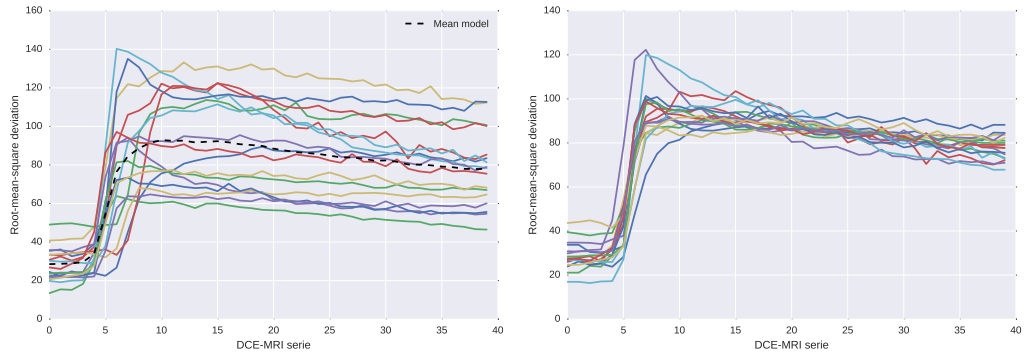
(a) RMSD computed for each patient of our dataset.

(b) RMSD after alignment using the curve parametric model.

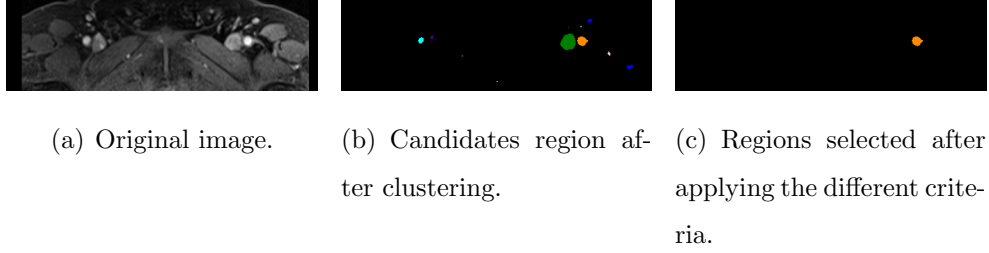Figure 4: Illustration of the correction of the time offset and the data dispersion.

(a) Original image.

(b) Candidates region after clustering.

(c) Regions selected after applying the different criteria.

Figure 5: Illustration of the segmentation of the area used to determine the AIF.

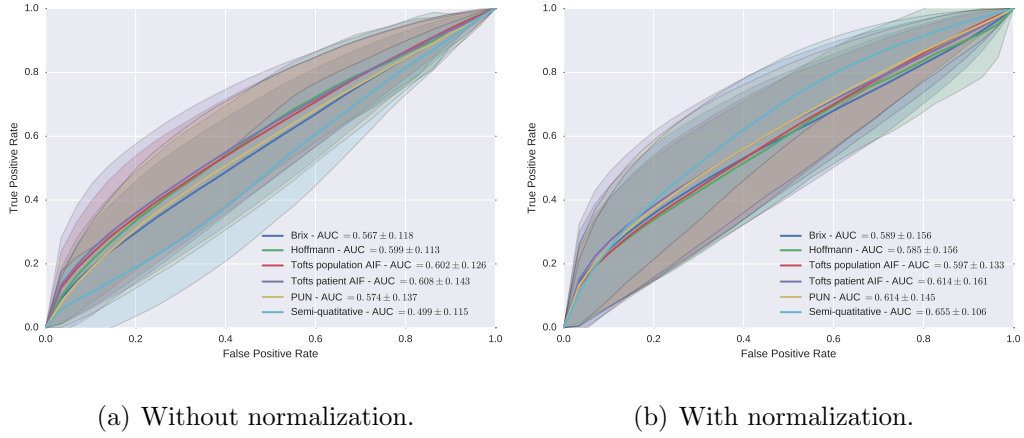(a) Without normalization.

(b) With normalization.

Figure 6: ROC analysis using a RF classifier with and without normalization DCE-MRI data for different pharmacokinetic models.
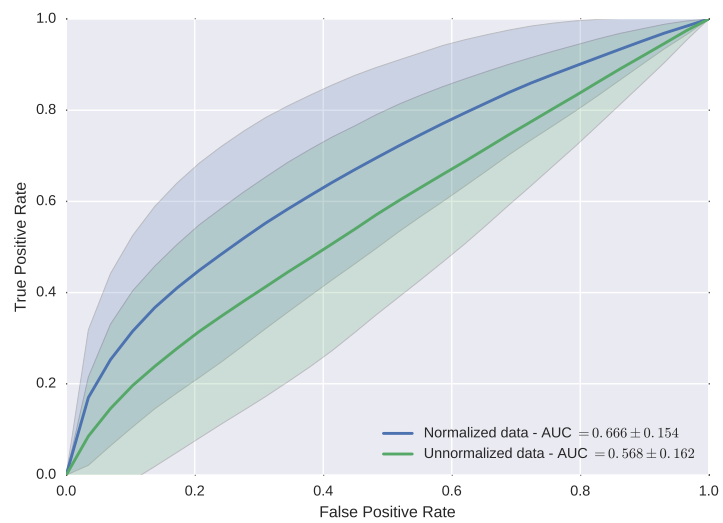
Figure 7: ROC analysis using the entire DCE-MRI signal with and without normalization in conjunction with a RF classifier.